STABILITY ANALYSIS OF FLAT-ELLIPTICAL GREENHOUSE SKELETON CONSIDERING INITIAL GEOMETRICAL IMPERFECTIONS
/
考虑初始几何缺陷的平椭圆管大棚骨架稳定性分析

Hengyan XIE[1,*], Cunxing WEI[2], Xin ZHENG[1], Wenbao XU[1]
[1] College of Civil Engineering and Water Conservancy, Heilongjiang Bayi Agricultural University, Daqing 163319, China;
[2] College of Engineering, Heilongjiang Bayi Agricultural University, Daqing 163319, China
Tel: +86-459-13766785587; E-mail: xiehy555@byau.cn
Corresponding author: Hengyan Xie
DOI: https://doi.org/10.35633/inmateh-76-31

Keywords: *flat-elliptical pipe greenhouse; initial imperfections; nonlinear buckling; full dynamic wind load; finite element analysis; structural stability*

ABSTRACT
This study investigates the nonlinear stability of flat-elliptical greenhouse skeletons under wind loads, accounting for initial imperfections. A finite element model was developed in ABAQUS, with nonlinear buckling analysis conducted via the arc-length method. Eigenvalue buckling analysis identified imperfection modes, and the impact of imperfection amplitudes on bearing capacity was assessed. Results showed that increasing imperfection amplitude decreased the ultimate bearing capacity, with a 461.2 N·m² capacity at L/300, and 520.26 N·m² at L/800. Initial imperfections notably influenced yield stages. This study demonstrates that considering initial imperfections provides a more accurate assessment of the skeleton's stability under extreme loads.

摘要
本研究研究探讨了在风荷载作用下，考虑初始缺陷的平面椭圆形温室骨架的非线性稳定性。通过 ABAQUS 建立了有限元模型，并采用弧长法进行非线性屈曲分析。特征值屈曲分析用于识别缺陷模式，并评估缺陷幅度对承载力的影响。研究结果表明，随着缺陷幅度的增加，最终承载力下降，在 L/300 情况下承载力为 461.2 N·m²，而在 L/800 情况下为 520.26 N·m²。初始缺陷显著影响了屈服阶段。研究表明，考虑初始缺陷能够更准确地评估骨架在极端荷载下的稳定性。

INTRODUCTION
In modern agriculture, greenhouses are essential for maintaining stable crop growth, particularly in regions with harsh or fluctuating climates. They offer controlled environments that improve yield and quality. The structural skeleton, as the main load-bearing system, is critical to a greenhouse's longevity, stability, and safety. Thus, investigating its mechanical behavior under complex loads holds significant theoretical and practical value.

Historically, bamboo served as the primary structural material until the 1950s, but its susceptibility to corrosion and degradation limited its durability. In the 1980s, hybrid structures combining bamboo and steel emerged to improve strength, yet corrosion at the interface remained problematic. With advancements in steel production and reduced costs in the 21st century, steel—particularly galvanized steel pipes with high corrosion resistance and load-bearing capacity—became the dominant material, markedly enhancing greenhouse performance and lifespan. Plastic greenhouses with different skeleton types as shown in Fig. 1.

a) Bamboo skeleton ***b) Bamboo-steel skeleton*** ***c) Steel skeleton***

Fig. 1 – Plastic greenhouses with different skeleton types

Hengyan Xie, Prof. Ph.D. Eng.; Cunxing Wei, Ph.D. Eng. Xin Zheng, Prof. Ph.D. Eng.; Wenbao Xu, Ph.D. Eng.

Steel structures, favored for their high strength and stiffness, resist external loads like wind and snow effectively while minimizing deformation. However, initial imperfections in steel components can compromise stability, often causing local or global buckling prior to reaching ultimate strength. These imperfections—defined by their location, shape, and evolution—are critical factors influencing failure modes. Nonlinear buckling analysis offers a more accurate evaluation of these effects, especially under complex or extreme load conditions. Cylindrical lattice shells, akin to greenhouse frames, have been extensively studied. For instance, Liu (2016) and Gu (2019) analyzed stochastic initial imperfections and their impact on buckling under various loads. Their findings underscore the necessity of including imperfections in structural analyses to ensure safety and performance reliability. Traditional analyses often assume ideal, defect-free models. Studies by *Ren (2019), Jiang (2021)*, and others employed finite element and time-domain methods to analyze stress and vibration responses in idealized skeletons. However, such simplifications may underestimate structural vulnerability under severe loads like heavy snow or strong winds, leading to significant instability and deformation.

Given the nonlinear nature of the loads acting on greenhouses, initial imperfections can exacerbate the risk of buckling and instability, affecting the long-term performance of the structure. Therefore, nonlinear buckling analysis of greenhouse skeletons, considering initial imperfections, is essential for a more accurate assessment of structural behavior under real-world loading conditions. Moreover, such analysis can reveal the impact of initial imperfection on the stability of the structure under extreme loads or adverse environmental conditions *(Cai, 2015; Zeng, 2024)*. While several studies have incorporated initial imperfections in the stability analysis of greenhouse skeletons, including the work by *Yu (2007) and Bao (2023)*, who performed nonlinear buckling analysis of arch-roof and Venlo-type greenhouses, there remains a gap in the research on the nonlinear buckling behavior of greenhouse skeletons under full dynamic wind loads. The specific mechanisms of structural instability in these conditions are not yet fully understood.

This study aims to fill this gap by assessing the stability of greenhouse structures under full dynamic wind load, highlighting potential instability risks induced by local buckling, and ultimately improving structural safety margins. The findings of this research will provide valuable theoretical support for the design, construction, and long-term operation of greenhouse structures, ensuring their safety and performance under extreme loading conditions.

MATERIALS AND METHODS

Analysis process

According to the code for design of steel structures *(GB50017-2017)* and the technical specification for space skeleton structures *(JGJ 7—2010)*, the impact of initial geometric imperfections, specifically the installation deviations from the intended curved surface shape, must be considered in the full-process analysis of lattice shell structures (skeletons). The distribution of initial geometric imperfections is typically represented by the lowest-order buckling mode of the structure, with the maximum value of the imperfection taken as 1/300 of the span of the lattice shell.

Based on these specifications, the following steps were taken to perform the nonlinear buckling analysis of the greenhouse skeleton structure:

(1) Finite Element Model Creation and Verification: A detailed finite element model of the greenhouse skeleton was established and verified to ensure its accuracy in simulating the structural behavior.

(2) Eigenvalue Buckling Analysis: A characteristic eigenvalue buckling analysis was conducted on the skeleton structure to determine the lowest-order buckling mode of the system.

(3) Simulation of Initial Geometric Imperfections: The distribution pattern of the initial geometric imperfections was simulated using the lowest-order eigenmode. The maximum value of the imperfections was set as 1/300 of the span of the greenhouse skeleton, as per the relevant design codes.

(4) Nonlinear Stability Analysis: A nonlinear stability analysis was performed using the arc-length method. The load-displacement curves and stability coefficients of the structure under different initial imperfections were compared to explore the influence of these imperfections on the stability of the structure.

Finite element model

In this study, a finite element model of a plastic greenhouse skeleton with 50 elliptical pipes was established using ABAQUS. The dimensional schematic of the skeleton is shown in Fig. 2.

As shown in Fig. 2, the structural span $L=10$ m; the structural height $H=3.6$ m; the rafter spacing $d=1$m.

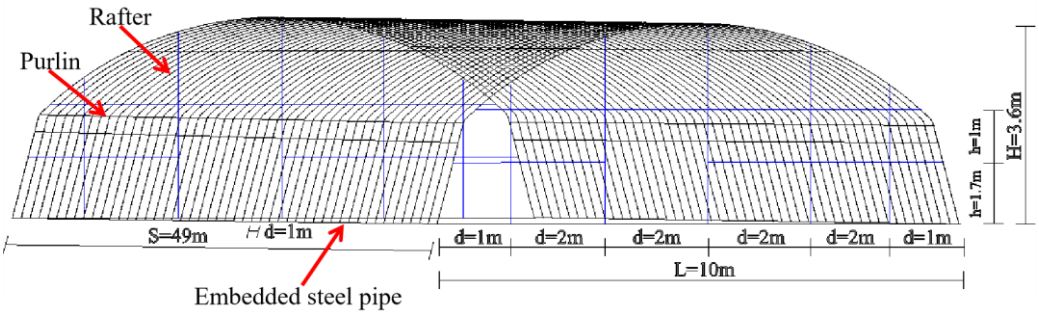

Fig. 2 – The dimensional schematic of the flat-elliptical pipe plastic greenhouse's skeleton

The material property parameters of the rafter, embedded steel pipe, and purlin are shown in Table 1.

Table 1

Material parameter of steel pipe

Material	*b*×*h* or *R* (mm)	*t* (mm)	ρ (kg/m³)	f_y (MPa)	λ	E (MPa)
Rafter	30×60	2	7.85	235	0.28	2.1×10^5
Embedded steel pipe	30×80	2	7.85	235	0.28	2.1×10^5
Purlin	ϕ 20	2	7.85	235	0.28	2.1×10^5

where: *b* is the width of section; *h* is the depth of section; *t* is thickness of section; *ρ* is density; f_y is the yield strength of steel; *λ* is Poisson ratio of steel; *E* is elasticity modulus of steel.

The C3D8R eight-node linear hexahedral element was selected to simulate the elliptical pipe greenhouse skeleton. The rafter was meshed according to its dimensions, with an approximate overall size set to 0.2, and each rafter was discretized into 2,380 elements. In actual engineering, the rafters and purlins are connected by clips, while the connections between the skeleton and the embedded steel pipe are welded. To improve computational efficiency, the connections between the rafters, purlins, and the embedded steel pipe were simplified to binding connections. This study applies full constraints between the two ends of the skeleton and the embedded steel pipe, restricting translational and rotational movements in all directions. For the other skeletons, hinged connections are used between the rafter and the embedded steel pipe.

Validation of the accuracy of the modeling method

Wang (2023) conducted a numerical analysis of a large-span pipe skeleton structure plastic greenhouse under the combined effects of dead load, wind load, live load, and crop load. Figure 3(a) shows the schematic diagram of the greenhouse skeleton model from the literature, while Figure 3(b) shows the finite element model established using the ABAQUS software in this study.

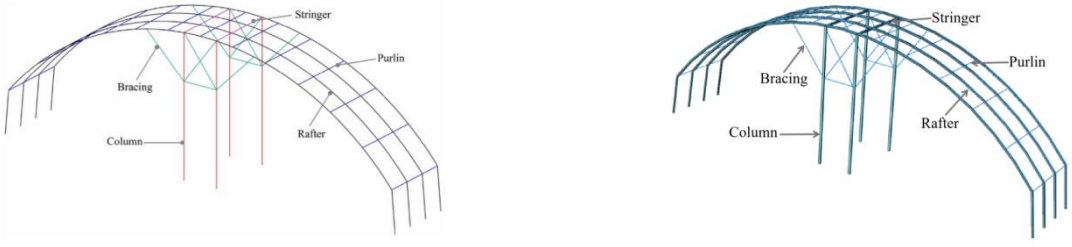

a) Literature ***b) Present***

Fig. 3 – Comparison of the structural diagrams of the greenhouse

To verify the accuracy of the modeling method, the validation model established in this study has the same material properties, skeleton dimensions, and boundary conditions as those in the original literature. All components are made of Q235 steel, with a yield strength of 235 MPa, Young's modulus of 206 GPa, Poisson's ratio of 0.3, and a density of 7850 kg/m³. The material is modeled using an ideal elastic-plastic constitutive relation. The rafter has a cross-section of a flat elliptical hollow pipe ($w\times h\times t=90\text{mm}\times40\text{mm}\times3\text{mm}$), while the columns have a rectangular hollow pipe cross-section ($w\times h\times t=90\text{mm}\times40\text{mm}\times3\text{mm}$).

The stringer also has a rectangular hollow pipe cross-section, with the same dimensions as the columns. The bracing has a circular hollow pipe cross-section ($d \times t = 32\text{mm} \times 2\text{mm}$), and the purlins have a circular hollow pipe cross-section as well ($d \times t = 25\text{mm} \times 1.5\text{mm}$). The bottom of the rafters and columns are set as fixed ends, restricting all degrees of freedom in all directions. The rafters and columns are connected with binding connections, and the connections between the bracing and the columns, rafters, and purlins are modeled as hinged.

In the literature, the greenhouse skeleton was modeled and analyzed using ANSYS software. In this study, the greenhouse skeleton was modeled and analyzed using the C3D8R solid element in ABAQUS finite element software. To verify the accuracy of the modeling method, displacement data at various points of the 1st and 2nd skeletons were extracted. The displacement data for the 1st and 2nd skeletons at each point are shown in Fig. 4.

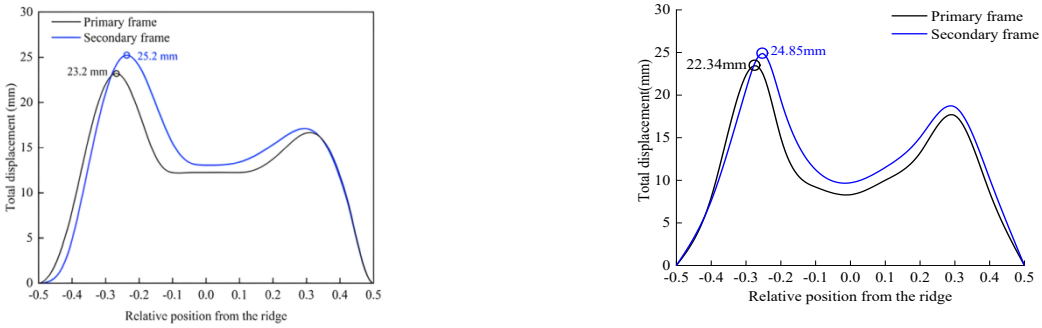

a) Literature result *b) Present result*

Fig. 4 – Comparison of the total displacement distribution curves

As shown in Fig. 10, the displacement variation trend calculated using the modeling method in this study is in good agreement with the displacement variation trend from the literature. In the literature, the maximum displacement of the 1st skeleton is 23.2 mm, while the modeling method in this study yields a maximum displacement of 22.34 MPa, with a relative error of 3.7%. For the 2nd skeleton, the maximum displacement in the literature is 25.2 mm, while the maximum displacement calculated in this study is 24.85 MPa, with a relative error of 1.38%. The results fall within a reasonable error range, indicating that the finite element modeling method used in this study is reliable.

Wind loads calculation

This study primarily investigates the nonlinear behavior of the steel skeleton under wind loads. Therefore, the structural load combination mainly consists of dead loads and wind loads. For simplicity, in the subsequent eigenvalue buckling analysis, the critical buckling load of the structure is determined by applying the dead and wind loads in the form of concentrated forces at each point of the skeleton, as shown in Fig. 5.

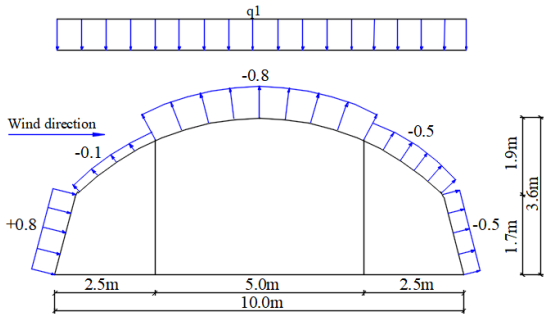

Fig. 5 – Shape coefficient on the flat-elliptical pipe skeleton plastic greenhouse

The plastic greenhouse studied in this study is located in Jiamusi City, Heilongjiang Province, China. According to the Chinese standard *GB/T51183-2016 (MOHUED, 2016),* the design service life of a plastic greenhouse is 10 years. Based on this code, the basic wind pressure in Jiamusi is 0.38 kN/m², which corresponds to the instantaneous wind speed with a duration of 3 seconds. On the other hand, according to the *Chinese standard GB/T50009-2012 (MOHUED, 2012),* the basic wind pressure in Jiamusi is 0.65 kN/m², which is based on the 10-minute average wind speed for a 50-year return period. The ratio of the 10-year return period wind pressure to the 50-year return period wind pressure is 0.734, thus the basic wind pressure for a 10-year return period with a 10-minute duration is 0.65 × 0.734 = 0.477 kN/m². After comparing the results from both codes, the basic wind pressure of 0.477 kN/m² was adopted in this study.

RESULTS AND DISCUSSION

Eigenvalue buckling analysis

First, the linear buckling analysis of the greenhouse skeleton structure was conducted using the finite element software ABAQUS, yielding the buckling modes and eigenvalues of the structure. Since initial imperfections are inevitably present in real structures, eigenvalue buckling analysis often overestimates the stability and load-bearing capacity of the structure. However, the linear buckling analysis provides an upper limit load value and initial imperfection distribution, serving as a basis for nonlinear buckling analysis.

The governing equation for eigenvalue buckling analysis is:

$$\left(\left[K_E\right]+\lambda\left[K_\sigma\right]\right)U=0 \tag{1}$$

where: $[K_E]$ is the elastic stiffness matrix of the structure; $[K_\sigma]$ is the geometric stiffness matrix of the structure; λ is the buckling factor, which is the eigenvalue, and U is the eigenvector matrix corresponding to each buckling factor, representing the buckling mode.

The eigenvalue buckling analysis of the greenhouse skeleton was conducted using ABAQUS finite element software under the action of dead load and wind load. The first 6 buckling modes and corresponding eigenvalues of the greenhouse skeleton are shown in Figure 6 and Table 2. To better visualize the buckling modes of the skeleton, the displacement has been amplified by a factor of 500 for easier observation.

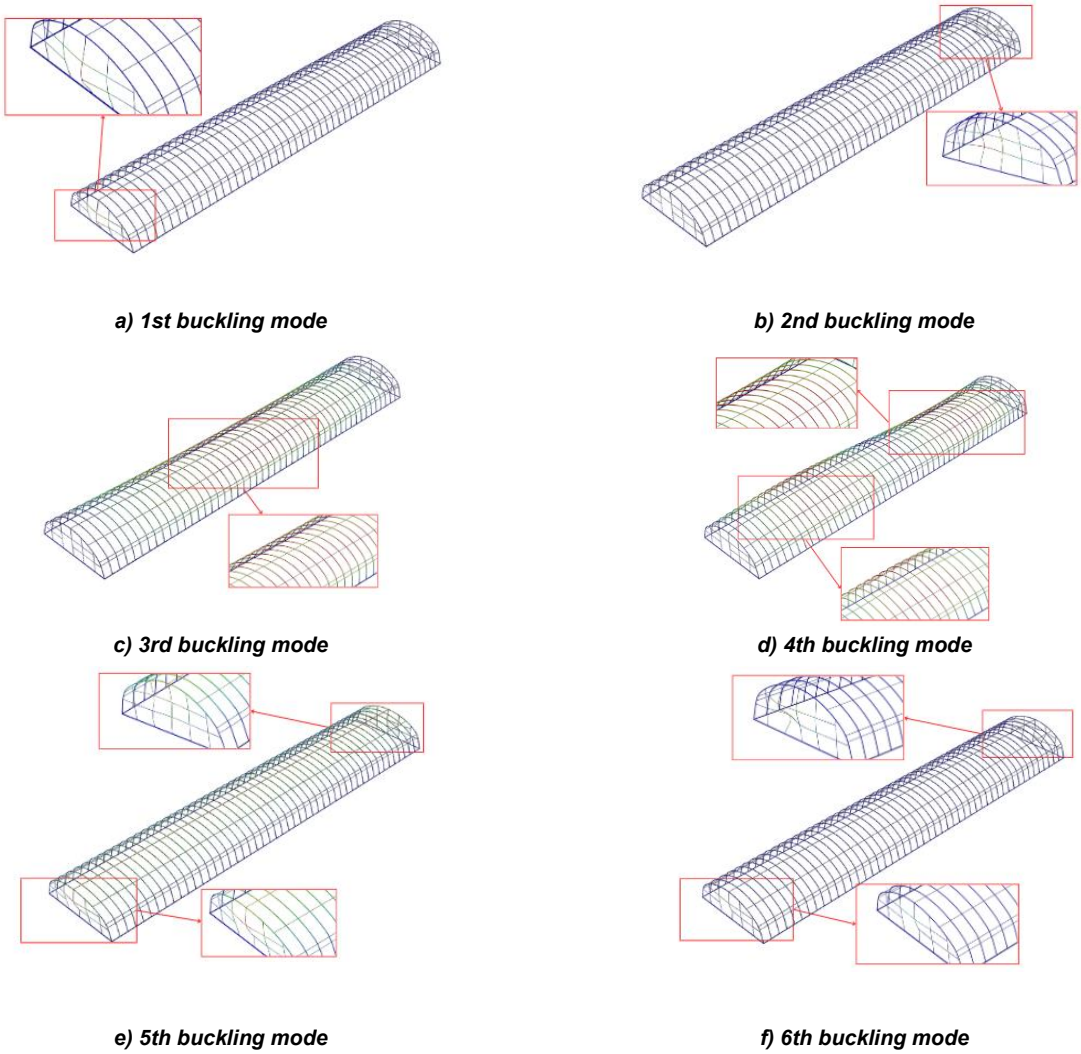

a) 1st buckling mode *b) 2nd buckling mode*

c) 3rd buckling mode *d) 4th buckling mode*

e) 5th buckling mode *f) 6th buckling mode*

Fig. 6 – The first 6 buckling modes of the skeleton structure

As shown in Figure 6, the first 2 modes of instability of the greenhouse skeleton structure occur in the sidewall areas. This is because, when the skeleton is considered as a whole, the skeletons on the sidewalls are weaker regions, causing the sidewall skeletons to experience instability first. The 3rd mode of instability exhibits an overall wave-like buckling, with the largest displacement observed near the central skeleton, where the structure bulges outward toward one side. The 4th mode of instability also shows wave-like buckling, but

the overall instability manifests as the skeletons near the two ends bulging outward in opposite directions. The 5th mode of instability is characterized by strip-like buckling, with localized instability occurring in the sidewall areas. The 6th mode, compared to the 5th, lacks the overall strip-like instability, and the instability is concentrated in the skeletons at both ends of the sidewalls.

Table 2

First 6 eigenvalues of the structure

Mode order	1st	2nd	3rd	4th	5th	6th
Eigenvalue	-25.1	-33.31	-35.43	-39.6	-41	-48.48

Nonlinear buckling analysis

According to the Technical specification for space frame structures *(JGJ 7—2010)*, the stability of the grid shell can be calculated using the finite element method considering geometric nonlinearity (i.e., load-displacement full process analysis). In the analysis, material behavior can be assumed to be elastic or elastic-plastic. In this study, both geometric and material nonlinearities are considered in the nonlinear buckling analysis of the structure. The first-order buckling mode of the skeleton structure is introduced as an initial imperfection into the greenhouse skeleton model, and a load-displacement full process analysis is performed. The iteration equation is as follows:

$$\left[K_t\right]\Delta U^{(i)} = F_{t+\Delta t} - N_{t+\Delta t}^{(i-1)} \tag{2}$$

where, $[K_t]$ is the tangent stiffness matrix of the structure at the current time step, $\Delta U^{(i)}$ is the iterative increment of the displacement at the current time step; $F_{t+\Delta t}$ and $N_{t+\Delta t}^{(i-1)}$ represent the external nodal load vector and the corresponding internal force vector of the structural members at the current time step, respectively.

For solving the above equation, various equilibrium path tracking methods can be used, such as the displacement increment method, load increment method, work increment method, residual energy method, and arc-length method. In this study, the Modified Riks method, commonly used for nonlinear buckling analysis in ABAQUS, is employed for solving. The constraint equation for the Modified Riks method is as follows:

$$(\Delta\bar{u})^T(\Delta\bar{u}) + \psi(\Delta\lambda)^2 = (\Delta l)^2 \tag{3}$$

where, ψ=1 represents the arc length increment for each iteration. An initial arc length must be specified, and during the calculation process, the arc length Δl is adjusted according to the specific problem to ensure both computational efficiency and accuracy.

In addition, during the loading process, the original geometry and shape of the structure will change due to the applied loads, causing the overall stiffness matrix to vary. Therefore, the linear equilibrium equation cannot effectively represent the behavior of the structure in the nonlinear process.

The linear equilibrium equation of the structure can be expressed as:

$$\left[K\right]u = F \tag{4}$$

where, $[K]$ is the overall stiffness matrix of the structure; u is the displacement vector of the structure; and F represents the external loads, which, for buckling problems, are typically the loads modified by the buckling load factor.

The updated overall stiffness matrix $[K]$ is commonly represented by the tangent stiffness matrix $[K_t]$, which is equivalent to the slope of the load-displacement curve. This type of nonlinear situation falls under the category of geometric nonlinearity. The tangent stiffness matrix is often used in the calculation of the equilibrium path to achieve rapid convergence. Its calculation is given by the following equation:

$$\left[K_t\right] = \left[K\right] + \left[K_\sigma\right] + \left[K_L\right] \tag{5}$$

where, $[K_t]$ is the tangent stiffness matrix of the structure at the current time step; $[K_L]$ is the initial displacement matrix.

In the absence of initial imperfections, the critical buckling load P_{cr} can be calculated using the Euler's buckling formula:

$$P_{cr} = \frac{\pi^2 EI}{L^2} \tag{6}$$

where, P_{cr} is the critical buckling load in the absence of imperfections; E is the Young's modulus; I is the moment of inertia of the cross-section; and L is the span of the structure.

The modified formula after introducing initial imperfections is as follows:

$$P_{cr}(\delta) = P_{cr}(1-\frac{\delta}{L}) \tag{7}$$

where, $P_{cr}(\delta)$ is the critical buckling load after introducing imperfections; δ is the initial imperfection amplitude.

The buckling analysis formula considering initial displacement imperfections, geometric nonlinearity, material nonlinearity, and the modified critical buckling load can be written as follows:

$$\left[K + K_{\sigma} + K_{L}\right]u + P_{cr}(1-\frac{\delta}{L})u = F \tag{8}$$

Nonlinear buckling analysis with initial imperfections was performed on the flat elliptical pipe greenhouse skeleton using the Riks method in ABAQUS finite element software. The load-displacement curves at the top of the middle rafter under different initial imperfections are shown in Fig.7.

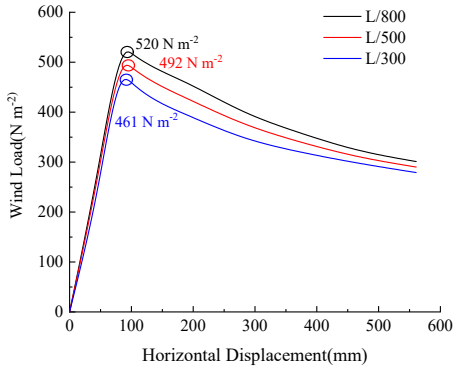

Fig. 7 – Load-displacement curves at the top of the middle rafter

As shown in Figure 7, when the load is small, the displacement increases in a linear trend. According to the technical specification for space frame structures *(JGJ 7—2010)* the first critical load value obtained from the full process analysis of the structure is taken as the ultimate load-bearing capacity of the structure. Therefore, when the maximum initial geometric imperfection amplitude is L/300, the ultimate bearing capacity is 461.2 N·m²; when the maximum initial geometric imperfection amplitude is L/500, the ultimate bearing capacity is 492.22 N·m²; and when the maximum initial geometric imperfection amplitude is L/800, the ultimate bearing capacity is 520.26 N·m². This shows that the ultimate bearing capacity of the structure decreases with the increase in the maximum initial geometric imperfection amplitude. This result is consistent with the conclusions previously drawn by *Xie and Chen (2015)*.

Comparison analysis of overall and local buckling of the skeleton

To investigate whether the post-buckling behavior of the structure meets the safety design requirements for steel structures, stress–displacement curves at various positions of the deformed skeleton were extracted. This analysis aims to clarify the impact of structural buckling on the stress distribution of individual members and to identify the most vulnerable positions within the skeleton. The displacement diagram of the skeleton structure, obtained through nonlinear buckling analysis, is presented in Fig. 8.

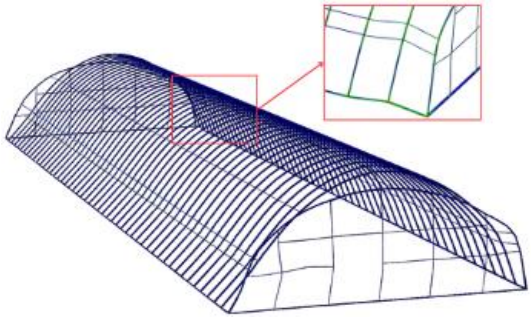

Fig. 8 – Displacement diagram of the skeleton structure

As shown in Fig. 8, the structure experiences significant overall buckling on the windward side, primarily manifesting as an overall strip-like instability. Meanwhile, on the leeward side, localized buckling deformation occurs at the end regions, primarily characterized by the arching of the steel pipes at the base, which induces deformation in both the skeleton and purlins. Therefore, this study will focus on analyzing the stress–displacement behavior of the components at both the localized buckling and overall buckling regions.

Stress analysis of rafter

The rafter, as the primary load-bearing components of the greenhouse skeleton, play a crucial role in supporting the structure under wind loads. Since wind loads primarily induce horizontal displacement in the structure, this study focuses on the variation of stress and horizontal displacement during the stress analysis. The Mises stress–horizontal displacement curves for the most unfavorable position of the rafter during the overall buckling and the local buckling of the structure were extracted and are shown in Fig. 9.

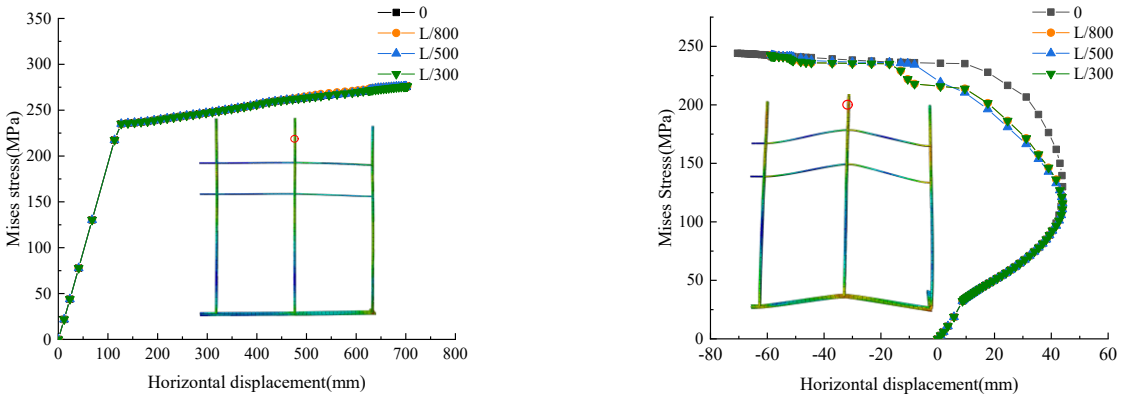

a) overall buckling *b) local buckling*

Fig. 9 – Most unfavorable position of Mises stress–horizontal displacement curves for rafter

As shown in Figure 9(a), when the horizontal displacement ranges from 0 mm to 150 mm, all curves exhibit a similar linear trend, indicating that initial imperfections have minimal impact on the structure's linear elastic behavior. During this stage, stress increases steadily, with a near-linear relationship between displacement and stress. As the displacement increases further, the structure enters the yielding stage, where the rate of stress growth slows. No significant differences are observed between curves with varying initial imperfections during this stage. From 200 mm to 700 mm horizontal displacement, the curves under different initial imperfection conditions stabilize, with minimal difference observed between the curves with and without initial imperfections (L/800, L/500, L/300). This suggests that, during overall buckling, initial imperfections have a relatively limited effect on the yield strength of the rafters, particularly in the linear-elastic stage.

In contrast, Figure 9(b) illustrates that the impact of initial imperfections becomes significant after local buckling. In the 0 mm to 40 mm displacement range, all curves show a near-linear increase, but as displacement reaches 40 mm, the curves diverge sharply. Samples with no initial imperfections show the highest yield stress, while increasing initial imperfections (L/800, L/500, L/300) cause the yield point to occur earlier and the yield strength to decrease. This indicates that initial imperfections considerably weaken the structure's resistance to yielding.

From 10 mm to -10 mm displacement, the gap between the curves narrows after reaching the yield point. In the range from -10 mm to -70 mm, the stress increase becomes more gradual, and the curve for the structure without initial imperfections exhibits a longer plateau, indicating greater plastic deformation capacity and higher ultimate load-bearing capacity.

Stress analysis of embedded steel pipe

The Mises stress–horizontal displacement curves at the most unfavorable position of the embedded steel pipe during the overall buckling and the local buckling of the structure were extracted and are shown in Fig. 10.

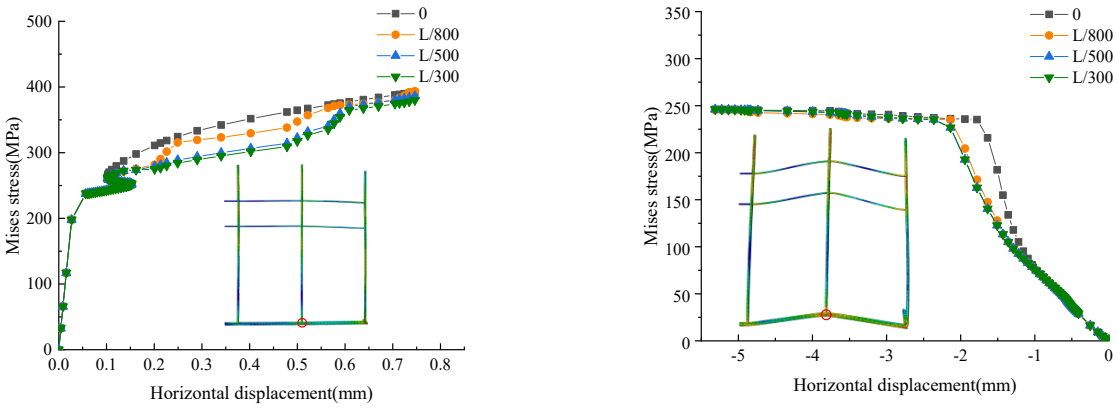

a) overall buckling *b) local buckling*

Fig. 10 – Most unfavorable position of Mises stress–horizontal displacement curves for embedded steel pipe

Figure 10(a) illustrates that within 0 mm to 0.06 mm of horizontal displacement, the curves exhibit a nearly identical linear trend, suggesting minimal impact of initial imperfections on the linear elastic behavior of the embedded steel pipe. Stress increases linearly, indicating stable elastic deformation. However, as the displacement progresses beyond 0.06 mm, the curves enter the yielding stage, where stress growth slows down. Between 0.1 mm and 0.6 mm displacement, the curves deviate from the linear relationship, displaying non-linearity. Notably, as initial imperfections increase, the curve flattens, reflecting a decrease in plastic deformation capacity and overall bearing capacity. This indicates that initial imperfections significantly weaken the yield strength and stability during overall buckling.

As shown in Fig. 10(b), from 0 mm to -1 mm displacement, the curves show a similar linear trend, again suggesting minimal impact of initial imperfections in the early stage. As displacement increases from -1 mm to -2 mm, the curves exhibit a nonlinear increase. The yield point varies significantly depending on initial imperfections, with structures without imperfections showing the steepest slope. From -2 mm to -5 mm displacement, the curves deviate further, entering the yield stage. The rate of stress increase slows, and significant differences emerge: without initial imperfections, the structure maintains higher yield strength and bearing capacity. However, with increasing initial imperfections (L/800, L/500, L/300), the yield point shifts earlier, and yield strength decreases, particularly under L/300 imperfections, highlighting the substantial reduction in load-bearing capacity.

Stress analysis of purlin

The Mises stress-horizontal displacement curves at the most unfavorable position of the purlin during the overall buckling and the local buckling of the structure were extracted and are shown in Fig. 11

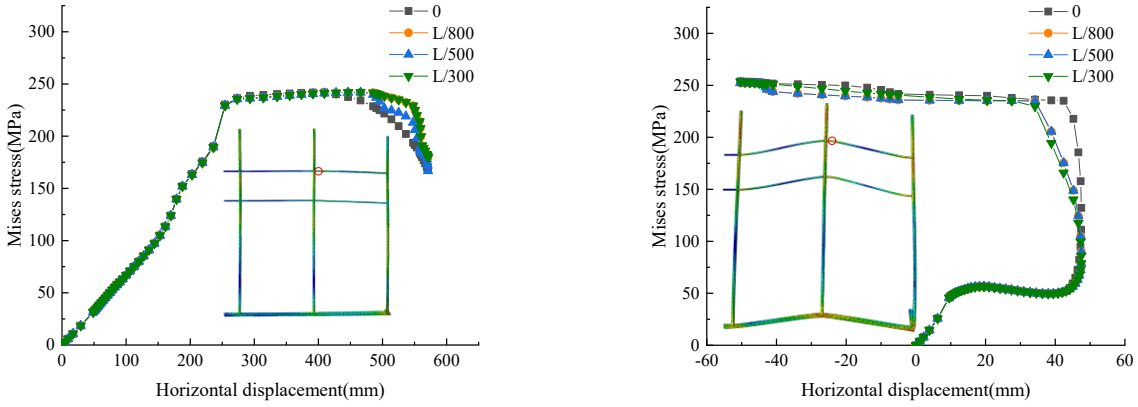

a) overall buckling *b) local buckling*

Fig. 11 – Most unfavorable position of Mises stress–horizontal displacement curves for purlin

As shown in Fig. 11(a), within the 0 mm to 100 mm horizontal displacement range, stress increases linearly, reflecting elastic deformation of the purlin. Initial imperfections have minimal impact during this phase. From 100 mm to 250 mm displacement, the curves show slight nonlinearity, with negligible differences between initial imperfection conditions, suggesting limited influence on the elastic behavior. As displacement reaches 250 mm to 450 mm, the purlin enters the yielding stage, characterized by a deceleration in stress increase. Curves for different initial imperfections level off, indicating stable plastic deformation. From 450 mm to 575 mm, stress sharply decreases as the purlin enters the necking stage. Notably, the curve without initial imperfections has a steeper slope, reflecting a weaker load-bearing capacity during the necking phase compared to those with initial imperfections (L/800, L/500, L/300).

Figure 11(b) reveals that the impact of initial imperfections becomes more significant after local buckling. In the 0 mm to 10 mm range, stress increases linearly, with minimal variation across curves. From 10 mm to 20 mm, the slope of the curves decreases, and from 20 mm to 50 mm, stress initially decreases before rising again. At 50 mm displacement, the curve without initial imperfections exhibits the steepest slope, indicating higher stiffness. The slope decreases with increasing imperfection size (L/800, L/500, L/300), highlighting a more pronounced effect of initial imperfections during the elastic stage of the purlin.

In summary, initial imperfections have a significantly different impact on the overall buckling and local buckling of the structure. In the case of overall buckling, initial imperfections have a relatively small effect on the rafters, embedded steel pipes, and purlins, especially during the elastic deformation stages, where the change in yield strength is minimal. However, as the horizontal displacement increases, the negative effects of the initial imperfections become more pronounced, primarily as the structure enters the yield and plastic stages. The yield point occurs earlier, and the yield strength significantly decreases, indicating a weakened ability to resist yielding.

CONCLUSIONS

In this study, an FEM model of the elliptical pipe greenhouse skeleton was established using ABAQUS software. The consistent imperfection method was employed to simulate the initial imperfections of the greenhouse skeleton, and the arc-length method was used to conduct nonlinear buckling analysis of the skeleton. The ultimate bearing capacity of the skeleton under different initial imperfection conditions was obtained. Stress analysis of various structural components at both overall and local buckling regions was performed. The following conclusions were drawn:

(1) The impact of initial imperfections on the rafters, embedded steel pipes, and purlins at the overall buckling positions is primarily concentrated in the yielding and plastic deformation stages. In contrast, the influence of initial imperfections at the local buckling positons on the rafters, embedded steel pipes, and purlins is not limited to the yielding and plastic stages; it also manifests significantly during the elastic stage. This results in a reduction in the structural stiffness and a decrease in the bearing capacity of the skeleton.

(2) When considering only the impact of initial imperfections, with the initial imperfection amplitude being L/300, the maximum displacement of the skeleton is approximately 1.33 times that of the skeleton without initial imperfections. Similarly, the maximum stress of the skeleton is approximately 1.11 times that of the skeleton without initial imperfections.

From the results of this study, it is evident that initial imperfections have a significant impact on the loading behavior of the greenhouse skeleton. After considering the effects of initial imperfections, both the displacement and stress of the skeleton increase significantly. Therefore, it is recommended that the design of such structures take into account the adverse effects of initial imperfections in order to enhance the structure's ability to resist wind loads.

ACKNOWLEDGEMENT

This study is supported by Natural Science Foundation of Heilongjiang Province of China (LH2019E072). All authors are grateful for this support.

REFERENCES

[1] Bao Z. (2023). Study on stability and seismic performance of Venlo greenhouse considering skin effect (考虑蒙皮效应的 Venlo 型温室稳定性及抗震性能研究). Master dissertation, *Sichuan Agricultural University*.

[2] Cai, J., He S., Jiang Z., Zhang Y., Liu Q. (2015). Investigation on maximum value of initial geometric imperfection in stability analysis of single layer reticulated shells (单层网壳结构稳定分析中初始几何缺陷最大值的研究). *Journal of Building Structures*. 36(06):86-92.

[3] Jiang Y., Bai Y., Wang C., Wang Y., Pang X. (2021). Dynamic response analyses of plastic greenhouse structure considering fluctuating wind Load. *Advances in Civil Engineering*. Vol. 2021, pp.1-13.

[4] Gu L., Gong J., Lu B. (2019). Influence of initial geometrical imperfections on overall stability of long-span truss string structure (初始几何缺陷对大跨张弦桁架结构整体稳定的影响研究). *Steel Construction*. Vol. 3, Issue 34, pp. 64-68.

[5] Liu Y., Cui X., Li Y., Hong H. (2021) Reliability analysis of stability of latticed shell structure considering initial geometric imperfections (考虑初始几何缺陷的网壳结构整体稳定性可靠度分析). *China civil engineering journal*. Vol. 54, Issue 7, pp. 12-23.

[6] Li, X., Wang C., Jiang Y., Bai, Y. (2022). Dynamic response analysis of a whole steel frame solar greenhouse under wind loads. *Scientific reports*. Vol. 12, Issue 5200, pp. 1-12.

[7] MOHURD (2017). *GB 50017-2017 Code for design of steel structures* (钢结构设计标准). Beijing, China: China Architecture & Building Press.

[8] MOHURD. (2016). *GB/T 51183-2016 Code for the design load of horticultural greenhouse structures*. (农业温室结构荷载规范) Beijing, China: China Planning Press. https://www.mohurd.gov.cn/gongkai/zhengce/zhengcefilelib/201702/20170214_230578.html

[9] MOHURD. (2010). JGJ7—2010 Technical specihcation for space frame structures (空间网格结构技术规程). Beijing, China.

[10] Ren, J., Wang, J., Guo, S., Li, X., Zheng, K., & Zhao, Z. (2019). Finite element analysis of the static properties and stability of a large-span plastic greenhouse. *Computers and Electronics in Agriculture*, Vol. 165, Issue 104957, pp.1-9.

[11] Wang C., Jiang Y., Xu Z., (2022). Ultimate bearing capacity of the solar greenhouse with hat-shaped steel under snow loads. *Transactions of the Chinese Society of Agricultural Engineering*, Vol. 38, Issue 19, pp. 172-179.

[12] Wang, C., Jiang, Y., Wang, T., Xu Z., Bai, Y. (2022). Analysis of wind-induced responses of landing assembled Chinese solar greenhouses. *Biosystems Engineering*, Vol. 220, Issue 6, pp. 214-232.

[13] Wang, C., Xu Z., Jiang, Y., Bai, Y., & Wang, T., (2023). Numerical analysis of static and dynamic characteristics of large-span pipe-framed plastic greenhouses. *Biosystems Engineering*, Vol. 232, Issue 6, pp. 67-80.

[14] Xie, H., Chen, B., & Chai, D. (2015). Ultimate load carrying capacity analysis of single-span arched plastic greenhouse frame (钢拱单栋塑料大棚平面内极限承载力分析). *Low Temperature Architecture Technology*, Vol. 37, Issue 8, pp. 46-49. https://doi.org/10.13905/j.cnki.dwjz.2015.08.018

[15] Yu Y., Wang J., Ying Y., (2007). Nonlinear finite element analysis of the bearing capacity of arch structure in plastic greenhouse on snow load working condition (塑料温室拱结构雪载工况下极限承载力的非线性有限元分析) *Transactions of the CSAE*, Vol. 23, Issue 3, pp. 158—162.

[16] Zeng Q., Zhu S., Yang X., Wu C., (2024). Research progress on simulation methods of initial geometric imperfection fields of single-layer gridshells (单层网壳结构初始几何缺陷场模拟方法研究进展). *Progress in Steel Building Structures*. Vol. 26, Issue 5, pp. 12-21.